

SCIENTIFIC REPORTS



OPEN

Highly responsive MoS₂ photodetectors enhanced by graphene quantum dots

Received: 03 March 2015

Accepted: 20 May 2015

Published: 03 July 2015

Caiyun Chen^{1,*}, Hong Qiao^{1,*}, Shenghuang Lin^{1,2,*}, Chi Man Luk², Yan Liu¹, Zaiquan Xu³, Jingchao Song³, Yunzhou Xue⁴, Delong Li⁴, Jian Yuan², Wenzhi Yu², Chunxu Pan⁴, Shu Ping Lau² & Qiaoliang Bao^{1,3}

Molybdenum disulphide (MoS₂), which is a typical semiconductor from the family of layered transition metal dichalcogenides (TMDs), is an attractive material for optoelectronic and photodetection applications because of its tunable bandgap and high quantum luminescence efficiency. Although a high photoresponsivity of 880–2000 AW⁻¹ and photogain up to 5000 have been demonstrated in MoS₂-based photodetectors, the light absorption and gain mechanisms are two fundamental issues preventing these materials from further improvement. In addition, it is still debated whether monolayer or multilayer MoS₂ could deliver better performance. Here, we demonstrate a photoresponsivity of approximately 10⁴ AW⁻¹ and a photogain of approximately 10⁷ electrons per photon in an *n-n* heterostructure photodetector that consists of a multilayer MoS₂ thin film covered with a thin layer of graphene quantum dots (GQDs). The enhanced light-matter interaction results from effective charge transfer and the re-absorption of photons, leading to enhanced light absorption and the creation of electron-hole pairs. It is feasible to scale up the device and obtain a fast response, thus making it one step closer to practical applications.

Layered transition metal dichalcogenides (TMDs, MX₂, M = Mo, W, Nb, Ta, Ti, Re; X = S, Se, Te) have attracted increasing attention as channel materials for field-effect transistors (FETs) because of their high electron mobility, excellent current ON/OFF ratio and low subthreshold swing^{1–6}. As a typical semiconductor from the family of TMDs, MoS₂ has a tunable bandgap that varies with thickness; that is, bulk MoS₂ has an indirect bandgap of 1.2 eV and, because of quantum confinement, monolayer MoS₂ has a direct bandgap of 1.8 eV^{1–3}. Atomically thin films of MoS₂ have excellent photoactive properties in terms of strong resonant light absorption (>20%) and high quantum luminescence efficiency^{4,7}, which makes these materials ideal for optoelectronic applications such as light emitting diodes^{8,9} and photodetectors^{10–15}.

The first phototransistor based on a mechanically exfoliated MoS₂ monolayer showed a photoresponsivity of only 7.5 mA W⁻¹ (Ref. 13) which is comparable to that of graphene-based devices (6.1 mA W⁻¹)¹⁶. The performance of phototransistor based on monolayer MoS₂ can be improved significantly because it possesses a high carrier mobility (up to approximately 410 cm²V⁻¹s⁻¹)¹⁷ and strong resonant absorption. By optimising the fabrication technique, photodetectors based on mechanically exfoliated monolayer MoS₂ can achieve an impressively high responsivity of 880 AW⁻¹ (Ref. 10). It should be noted, however, that multilayer MoS₂ has a density of state that is three times higher than monolayer MoS₂¹⁸, as well as

¹Institute of Functional Nano and Soft Materials (FUNSOM), Jiangsu Key Laboratory for Carbon-Based Functional Materials and Devices, and Collaborative Innovation Center of Suzhou Nano Science and Technology, Soochow University, Suzhou 215123, P. R. China. ²Department of Applied Physics, The Hong Kong Polytechnic University, Hung Hom, Hong Kong SAR, China. ³Department of Materials Engineering, Monash University, Clayton, VIC 3800, Australia. ⁴School of Physical and Technology, Wuhan University, Wuhan 430072, P. R. China. *These authors contributed equally to this work. Correspondence and requests for materials should be addressed to Q. B. (email: qlbao@suda.edu.cn)

a wider spectrum response¹² because of its narrower bandgap, which could afford effective broadband detection. Because it is still challenging to grow large area monolayer MoS₂ via chemical vapour deposition (CVD), the use of multilayer MoS₂ films as the channel material in phototransistors is likely to be a more practical solution, mainly because the growth of large area multilayer MoS₂ films on different substrates is quite successful^{19–22}. Nevertheless, the indirect bandgap of multilayer MoS₂ film intrinsically limits the photoresponsivity and photogain of such photodetectors.

In this work, we hybridised a multilayer MoS₂ film with QDs to create a new channel material for photodetection where the QDs function as an effective gain material. High quality and large area multilayer MoS₂ films were grown on SiO₂/Si substrates by the reaction of gaseous MoO₃ and sulphur via atmospheric pressure chemical vapour deposition (APCVD). This growth technique affords a simple device fabrication process that does not require material transfer. Because of fewer defects and impurities, multilayer MoS₂ films demonstrate surprisingly good performance for photodetection, which is comparable to the best record achieved on mechanically exfoliated MoS₂¹⁰.

To explore the performance limit of this material, we modified the MoS₂ thin film by incorporating nitrogen-doped graphene quantum dots (GQDs), which possess strong light absorption, long carrier lifetime and a sizable bandgap upon excitation^{23–26}. An *n-n* type van der Waals heterostructure consisting of GQDs and MoS₂ is formed, where the photoexcited holes can be induced successfully by MoS₂ and are subsequently trapped because of a small energy barrier in the heterojunction. The long carrier lifetime of the GQDs will cause the photoexcited carriers to recirculate several times at the interface. Moreover, light emission from the GQDs will be re-absorbed by MoS₂ to generate additional photo-carriers. Consequently, the MoS₂-GQDs hybrid system is an extremely efficient photoelectrical material that can achieve impressive photodetection performance. Indeed, this material ushers in an innovative approach for fabricating highly responsive and low cost photodetectors for practical applications.

Results and Discussion

We use the CVD method to controllably synthesise large area MoS₂ films on SiO₂/Si substrates. Details of the experimental setup and growth process are provided in the Methods and Supporting Information (Fig. S1). Figure 1a schematically illustrates the chemical reaction on a SiO₂ substrate for the production of MoS₂. Briefly, MoO₃ is largely reduced by sulphur vapour to form MoO_{3-x} species, which are further sulphurised and accompanied by the formation of MoS₂ on the SiO₂ substrate^{7,21}. The growth of MoS₂ follows a typical two-dimensional growth mode consisting of nucleation, growth and coalescence, as shown in Fig. 1b–d. The dark contrast in the images corresponds to MoS₂ crystals, and the surrounding area with bright contrast is the SiO₂ substrate. It is found that shorter growth times (*e.g.*, 5 min, Fig. 1b) will produce several atomically thin MoS₂ crystals with lateral sizes of 1–3 μm. Prolonging the growth time leads to an increase of nuclei density and a thicker layer. As a result, the newly grown MoS₂ crystals grow larger and coalesce with each other (Fig. 1c). Eventually, a continuous film is formed with an even longer growth time (*e.g.*, 30 min, Fig. 1d). The uniform contrast in the optical image (Fig. 1e) over a large area suggests that the MoS₂ thin film is continuous and uniform.

In the MoS₂ layered structures, each layer has a thickness of 6–7 Å^{1,27}. It is found that our samples are predominately 1–3 atomic layers thick. Atomic force microscopy (AFM) images (Fig. 1f) further confirm the number of layers of the MoS₂ film, in which the thickness of the MoS₂ trilayer is measured to be approximately 1.98 nm. Further characterisation of the thickness of monolayer and bilayer MoS₂ is presented in the Supporting Information (Fig. S2). Figure 1g shows a transmission electron microscopy (TEM) image of a MoS₂ film. The number of layers in the MoS₂ film can be determined by counting the dark fringes of the folded edges (inset of Fig. 1g). High-resolution transmission electron microscopy (HRTEM) is also employed to reveal the atomic lattice of the MoS₂ film, as shown in Fig. 1h. The selected area electron diffraction (SAED) pattern (inset of Fig. 1h) shows multiple six-fold symmetry spots, indicating that the MoS₂ film contains several grains possessing different crystal orientations. The HRTEM image of the GQDs (Fig. 1i) shows that the size of the GQDs is approximately 3–5 nm, where the in-plane lattice with a space of 0.25 nm is clearly resolved²⁵.

Spectroscopic characterisations are performed to systematically study the quality and uniformity of the MoS₂ film. Figure 2a shows the Raman spectra obtained from different locations on as-grown MoS₂ films with different thicknesses. Two characteristic peaks, which correspond to the *E*_{2g}¹ and *A*_{1g} vibrational modes^{28–30}, are observed. The difference (Δ) between these modes in the as-synthesised MoS₂ monolayer is approximately 20.6 cm⁻¹, which is slightly larger than the mechanically exfoliated monolayer MoS₂ because of crystalline imperfections. The peak differences (Δ) of bilayer and trilayer MoS₂ are 21.4 and 23.1 cm⁻¹, respectively, which are consistent with a previous report²⁹. As the number of layers increases, it is found that the *E*_{2g}¹ peak redshifts whereas the *A*_{1g} peak blueshifts obviously. This observation is attributed to columbic interactions and possible stacking-induced changes in the intra-layer bonding²⁸. Additionally, we also captured the Raman image of MoS₂ by integrating the *A*_{1g} peak to verify the thickness uniformity, as shown in Fig. 2b. This figure clearly reveals that the intensity of the *A*_{1g} peak, which scales linearly with the thickness, is homogeneous over the entire scanning area (approximately 20 μm).

Figure 2c shows the UV-visible absorption and photoluminescence (PL) spectra of the MoS₂ film. Two absorption peaks at approximately 620 nm and 670 nm are observed, which correspond to direct excitonic transitions at the Brillouin zone *K* point in MoS₂⁴. Correspondingly, the PL spectrum depicts two feature peaks located at 620 nm and 670 nm, respectively. The PL mapping result (Fig. 2d) suggests that

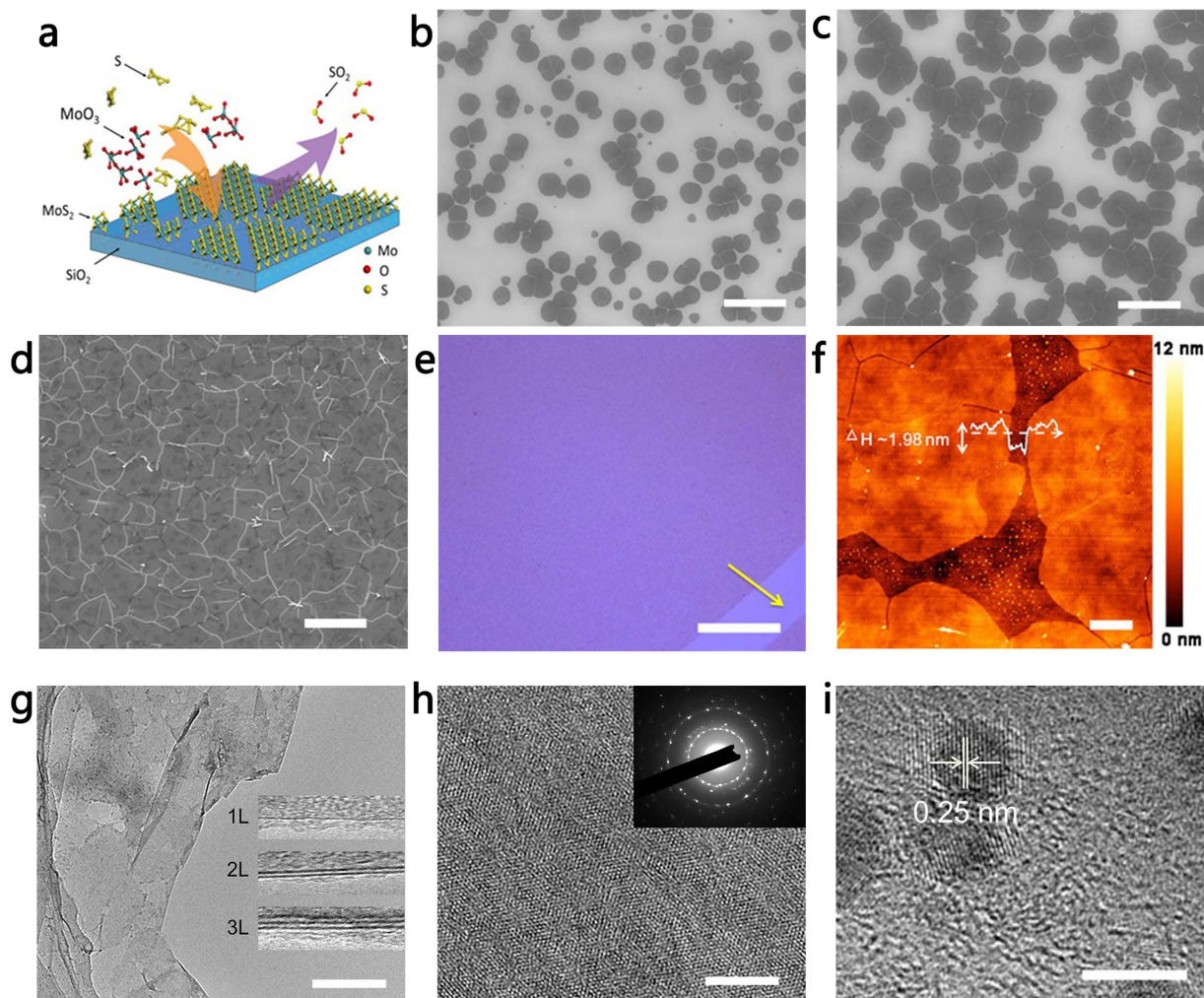


Figure 1. Material characterisations of MoS₂ and GQDs. (a) Schematic diagram showing the chemical reaction on a SiO₂ substrate for the production of MoS₂. (b–d) SEM images showing different growth stages of MoS₂ with reaction times of 5, 10 and 30 min, respectively. Scale bars in (b–d): 20 μm. (e) Optical image of MoS₂ on a SiO₂ substrate. The yellow arrow indicates a scratch. Scale bar: 50 μm. (f) AFM topography of a MoS₂ film on a SiO₂ substrate. The white profile indicates three atomic layers. Scale bar: 1 μm. (g) TEM image showing a folded MoS₂ film. Scale bar: 200 nm. The inset shows the folded edges of monolayer (1L), bilayer (2L) and trilayer (3L) MoS₂ films. (h) HRTEM image of a MoS₂ film. The scale bar is 5 nm. The inset shows the corresponding electron diffraction pattern. (i) HRTEM image of GQDs. Scale bar: 2 nm.

the MoS₂ film is relatively uniform. The X-ray photoelectron spectroscopy (XPS) result in Fig. 2e clearly depicts the Mo-related peaks (*i.e.*, Mo-3d_{3/2} at 232.9 eV and Mo-3d_{5/2} at 229.9 eV) and the S-related peaks (*i.e.*, S-2p_{1/2} at 163.9 eV and S-2p_{3/2} at 162.7 eV), which are consistent with the reported values for MoS₂ crystals^{20,31}. If we compare the integration area of these two sets of peaks, we are able to conclude that the atomic ratio of Mo and S is close to 1:2. Figure 2f shows the UV-visible absorption and PL spectra of GQDs. It is found that the GQDs possess an absorption peak at 283 nm and a broad PL peak from 450 nm to 700 nm. These results are similar to previously published reports^{24,25}.

Figure 3a depicts the device photoresponse modulated by light power at an excitation wavelength of 405 nm. We can clearly see that the device drain current (I_d) demonstrates enhancement under light illumination and that it increases at higher light power. At an excitation power of 30.1 μW, the device drain current reaches 10.15 μA when the source-drain voltage $V_{ds} = 1.68$ V, which is 1000 times higher than the current in the dark state (*i.e.*, at 11 nA). Such a high optical ON-OFF ratio is comparable to the highest ratio reported for single or multilayer MoS₂ phototransistors^{10,12}. Moreover, our device demonstrates high sensitivity that is responsive to very weak light (5 nW, Fig. S4). However, the device response is quite slow (with rise and decay times longer than 50 s). This slow response is likely caused by either defects or charge impurity states inside the bandgap or by the presence of trap states between MoS₂ and the underlying SiO₂ layer, which usually occurs for MoS₂ grown with the CVD method^{10,11,32}.

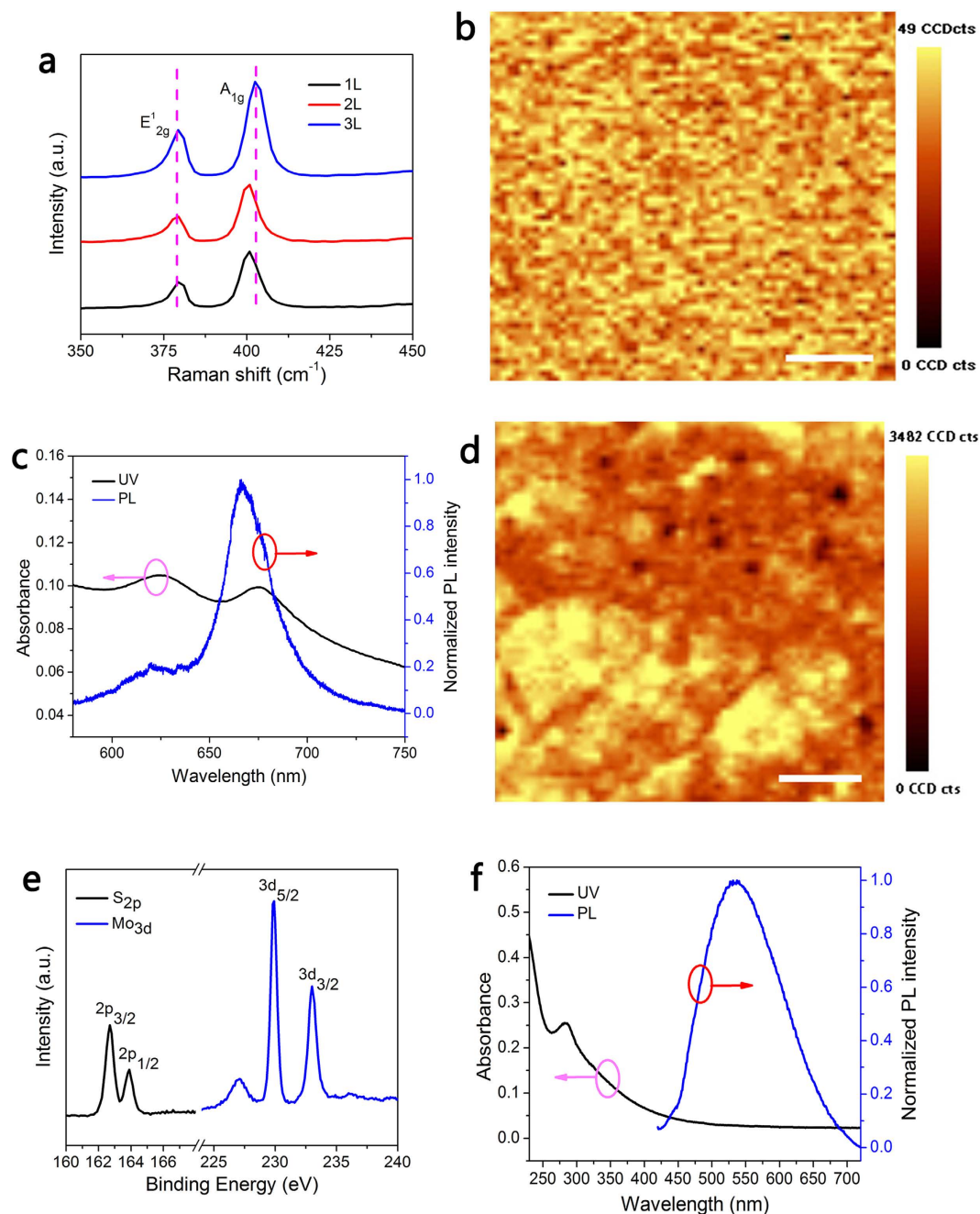


Figure 2. Spectroscopic characterisations of MoS₂ films. (a) Raman spectra of as-grown monolayer (1L), bilayer (2L) and trilayer (3L) MoS₂ on SiO₂/Si substrates. (b) Raman image of the characteristic peak (A_{1g}) integrated from 395 to 410 cm⁻¹. Scale bar: 4 μm. (c) PL and UV-visible spectra of a multilayer MoS₂ film. (d) PL image of the characteristic peak at 670 nm obtained by integrating from 610 to 710 nm. Scale bar: 4 μm. (e) X-ray photoelectron spectroscopy (XPS) spectra of a thin MoS₂ film. (f) PL and UV-visible spectra of GQDs.

Figure 3b shows the corresponding photocurrent and photoresponsivity curves as functions of incident power. It is noteworthy that the photocurrent increases exponentially while prompting the light power, whereas the responsivity drops exponentially. This effect might be related to the multifaceted generation, separation and transport processes of photoexcited carriers³³, and might also be caused by the trap states inside multilayer MoS₂ or between MoS₂ and the SiO₂ substrates^{10,11,32}. The photocurrent generation can be explained by the energy diagram in Fig. 3c. Here, a typical metal-semiconductor contact between MoS₂ and the Au electrodes indicates the band bending at the interface. An energy barrier hinders the carrier injection from the electrodes under dark conditions. However, electrons inside the valence band (VB) can be easily excited to the conduction band

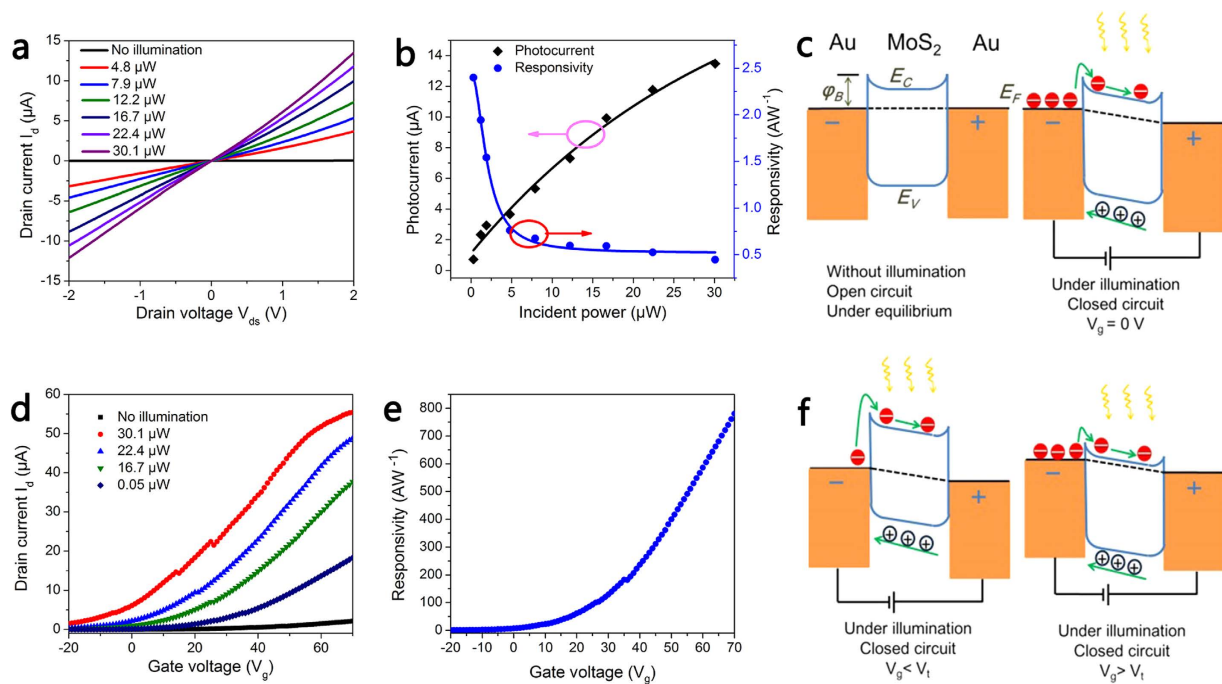


Figure 3. Optoelectronic characterisations of a multilayer MoS₂ phototransistor. (a) Device drain current (I_d) as a function of source-drain voltage (V_{ds}) for an excitation wavelength of 405 nm with different incident powers. (b) The dependence of photocurrent and photoresponsivity on incident power. The blue and black dots are the original data, whereas the lines are the exponential curves. (c) Schematic energy diagram of the device without and with illumination showing the energy barrier and photocurrent generation process. There is a non-zero source-drain bias ($V_{ds} \neq 0$ V), but the gate bias is kept at zero ($V_g = 0$ V). (d) Device drain current as a function of gate voltage under different illumination powers. Source-drain bias: $V_{ds} = 1$ V. (e) The photoresponsivity versus back gate voltage. Source-drain bias: $V_{ds} = 1$ V; light power: 50 nW. (f) Schematic energy diagram showing photocurrent generation processes with different gate bias ($V_g < V_t$ and $V_g > V_t$). There is a non-zero source-drain bias.

(CB) by photons when the device is biased and exposed to incident light, which will greatly increase the concentration of transported carriers.

The multilayer MoS₂ phototransistor has good gate tunability, which shows higher drain current at higher gating voltage, as shown in Fig. 3d. These results clearly show that the drain currents of both the OFF and ON states increase dramatically under light illumination. With a positive gate voltage (e.g., $V_g = 70$ V), the device can generate a photocurrent as high as 16.2 μ A, even at a very low excitation light power of 50 nW. The photoresponsivity is estimated to be on the order of 10^2 AW^{-1} while the gate bias is applied, as shown in Fig. 3e. The highest photoresponsivity is 800 AW^{-1} ($V_g = 70$ V), which is comparable to the best reported performance of a phototransistor based on monolayer or multilayer MoS₂^{10,12,13,15}. The gate modulated photocurrent can be well understood by the energy diagram in Fig. 3f. Depending on the relationship between the gate bias (V_g) and the threshold voltage (V_t), the Fermi level in MoS₂ can be shifted up ($V_g > V_t$) or down ($V_g < V_t$) while sweeping the back gate voltage, which results in the ON or OFF switch of the phototransistor.

With the aim to further increase the photoresponsivity and shorten the response time, *n*-doped GQDs were hybridised with MoS₂ to form a heterostructure device, as shown in Fig. 4a. The dramatic change in the transfer characteristics of the MoS₂-GQDs phototransistor is noteworthy, as shown in Fig. 4b. The threshold voltage shifts to a lower voltage and the drain current increases by 60 times for the ON state. From the *I*-*V* characterisations shown in Fig. 4c, we can see that the MoS₂-GQDs phototransistor has a much larger drain current under illumination, which is approximately 5 times higher than a pure MoS₂-based phototransistor. Time-dependent photoresponse measurements have also been performed, as shown in Fig. 4d. Here, we can see that the device rise time is significantly reduced from 20 s to 70 ms following the incorporation of GQDs. It is proposed that the drain current increasing rate ($\Delta I_{ph}/\Delta t$) is caused by the increased carrier concentration. Another interesting phenomenon is that the fall times of the drain current, both τ_1 and τ_2 , are reduced by a factor of ten. It is generally believed that the fast decay time component τ_1 is related to the direct recombination of photoexcited carriers and that the slow decay time component τ_2 is caused by sub-bandgap emissions resulting from the charge impurity and trap

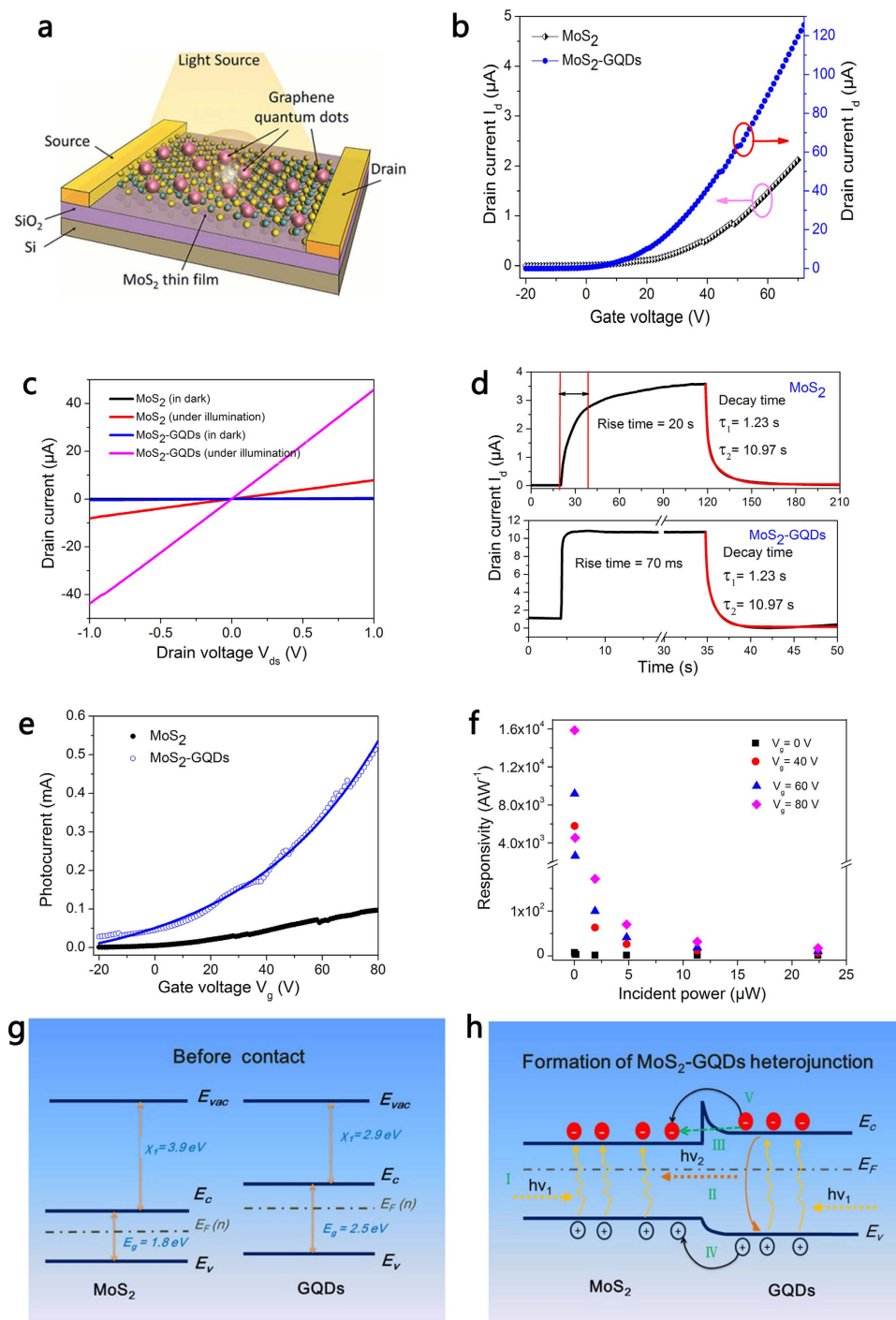


Figure 4. Optoelectronic characterisations of a MoS₂-GQDs phototransistor. (a) Schematic of a MoS₂-GQDs heterostructure phototransistor. (b) Typical transfer curves of MoS₂ and MoS₂-GQDs transistor devices. I_d : drain current. Source-drain voltage: $V_{ds} = 1$ V. (c) Drain current (I_d) as a function of source-drain voltage (V_{ds}) without and with light illumination for MoS₂ and MoS₂-GQDs phototransistors. Laser wavelength: 405 nm; light power: 17 μ W. (d) Time-dependent photoresponse of MoS₂ (top) and MoS₂-GQDs (bottom) devices. (e) Photocurrent as a function of back gate voltage for MoS₂ and MoS₂-GQDs devices. Incident light power: 30.1 μ W. The blue and black dots are the original data; the blue line is included for clarity. (f) The dependence of photoresponsivity on incident light power under back gate modulation. (g) Energy diagram of MoS₂ and GQDs before contact. (h) Energy diagram of the interface between MoS₂ and GQDs after the formation of a heterojunction. Five photoelectrical processes are proposed: I, Photon excitation in MoS₂ and the GQDs; II, Re-absorption of the emitted photons from the GQDs by MoS₂; III, Electrons tunnelling from the GQDs to MoS₂; IV, Hole transfer from the GQDs to MoS₂; V: Thermal excitation of electrons from the GQDs to MoS₂.

states inside the bandgap of MoS₂^{11,32}. The greatly shortened decay time is related to the efficient charge transfer between MoS₂ and the GQDs.

Relative to a MoS₂-based phototransistor, the MoS₂-GQDs phototransistor has a superior gate tunability in terms of higher photocurrent, as shown in Fig. 4e. The photocurrent of our MoS₂-GQDs device can be effectively modulated by the back gate voltage, and the photocurrent value can reach as high as 0.55 mA under an adequate gate bias ($V_g = 80$ V), which is 5 times that of a MoS₂ device. Figure 4f shows the dependence of device photoresponsivity on incident light power under different back gate biases. Similar to a thin film MoS₂ device, the responsivity decreases exponentially as the light power increases, and the maximum responsivity is 1.6×10^4 AW⁻¹ under an excitation power of 50 nW ($V_g = 80$ V), which is two orders of magnitude higher than a pure MoS₂ device, and among the highest responsivity recorded for MoS₂ photodetectors^{10,12}.

To further evaluate the performance of the device, we calculated the photoconductive gain using $G = \frac{\tau}{t_L}$, where τ is the carrier life time extracted from the current decay curve (Fig. 4d, $\tau = \tau_2 = 1.10$ s) and t_L is the carrier transit time. The carrier transit time can be calculated by $t_L = \frac{L^2}{\mu V_{ds}}$, where L is the channel length ($L = 20 \mu\text{m}$ for our devices), μ is field effect carrier mobility and V_{ds} is source-drain voltage. The carrier mobility μ can be extracted from the device transfer curve shown in Fig. 4b using the equation $\mu = \frac{1}{V_{ds}} \frac{\partial I_D}{\partial V_g} \frac{dL}{\epsilon W}$, where ϵ is the dielectric constant of SiO₂, d is the thickness of SiO₂ ($d = 300$ nm), and W is the channel width. Accordingly, we can determine a photoconductive gain up to approximately 2.4×10^7 , which is comparable to other reported atomically thin graphene-MoS₂ heterostructure phototransistors^{34,35} and graphene-QDs hybrid photodetectors³³.

To understand the influence of GQDs on the MoS₂ device and the mechanism of photocurrent generation, we propose a schematic energy band diagram, as illustrated in Fig. 4g,h. As both MoS₂ and GQDs are semiconductors with sizable bandgaps, it is important to establish the relative energy levels to determine the band bending and carrier transfer direction when they interact with each other. According to previous reports^{10,36–38}, the electron affinity of few-layered MoS₂ is approximately 3.9 eV, which is larger than that of GQDs (2.9 eV)³⁹. Because our multilayer MoS₂ film possesses 2–3 atomic layers, we assume its bandgap is close to that of the monolayer MoS₂ (1.8 eV)¹⁰ and much smaller than the bandgap of GQDs (4.5 eV)³⁹. Furthermore because these two materials are both *n*-type doped, we propose an energy diagram before the formation of the heterojunction (Fig. 4g). It is clear that the Fermi level of GQDs is closer to the vacuum level than the Fermi level in MoS₂. When MoS₂ and the GQDs contact and form a van der Waals heterostructure, the formation of the Fermi level between these materials leads to an injection of electrons from the GQDs to MoS₂, which is evidenced by the left shift of the threshold voltage in the electrical transfer curve shown in Fig. 4b. The movement of electrons causes the band bending³⁶, as shown in Fig. 4h, which manifests as a small energy barrier.

The light-matter interaction in the MoS₂-GQDs heterojunction is complicated, as both of these two materials strongly absorb and emit light. It is proposed that at least five photoelectrical processes are involved, as schematically illustrated in Fig. 4h. According to the steady state PL measurements (Fig. S7), it is notable that the PL of the GQDs is almost quenched whereas the PL of MoS₂ is maintained. We suggest that a re-absorption of emitted photons (process II) from the GQDs by MoS₂ is the origin of the PL quenching. Furthermore, this process will induce new electron-hole pairs, which in return serve as charge carriers to increase the photocurrent. Moreover, the photoexcited electrons in the valence band of the GQDs may be injected into MoS₂ through a tunnelling process (process III), which will also contribute extra electrons to increase the photocurrent. The time-resolved PL decay transients show that the decay time of MoS₂-GQDs is decreased to 85 ps, which is much shorter than the decay times of MoS₂ (224 ps) and GQDs (337 ps) (Fig. S7). This indicates that the recombination rate is faster in MoS₂-GQDs, which results from the transfer of holes from GQDs to MoS₂ (process IV) and is stimulated by an endogenous electrical field. Consequently, the photoresponse is faster in MoS₂-GQDs photodetectors, as evidenced in Fig. 4d.

Conclusions

In summary, highly responsive photodetectors based on the hybrid of MoS₂ and GQDs have been demonstrated, which have a photoresponsivity of 1.6×10^4 AW⁻¹ and a photogain of 2.4×10^7 . The incorporation of GQDs into MoS₂ forms an *n-n* type heterostructure with significantly improved carrier mobility on account of the injection of electrons from the GQDs to MoS₂. The improved photodetection performance is attributed to enhanced light-matter interactions resulting from the tunnelling of photoexcited carriers from the GQDs to MoS₂, the re-absorption of emitted photons from the GQDs by MoS₂ and the transfer of holes from the GQDs to MoS₂. Our work demonstrates an effective and applicable way to optimise the photodetection performance of MoS₂ and other analogous two-dimensional TMD materials.

Methods

Growth of the MoS₂ films and GQDs. The MoS₂ films were grown directly on a SiO₂/Si substrate in a 2-inch quartz tube. High purity MoO₃ powder (99.5%, Alfa Aesar) and sulphur (99.5%, Sinopharm Chemical Reagent Shanghai Co., Ltd) were used as the precursors. The sulphur powder was placed outside the hot zone and mildly sublimated by heating belts at 140 °C. The distance between the sulphur

and MoO₃ was approximately 25 cm. The SiO₂/Si substrates were placed downstream along the MoO₃ source. Argon (99.999%) was used as the carrier gas to convey MoO_{3-x} onto the SiO₂/Si substrates. The tube was flushed with argon to maintain normal pressure. The growth conditions were 700 °C for 30 min with an argon gas flow rate of 50 standard-state cubic centimetres per minute (sccm). The GQDs were synthesised following a previously reported methodology²⁵.

Characterisation of the MoS₂ films. The MoS₂ films were wet-transferred onto a quartz substrate by etching away the SiO₂ in a potassium hydroxide solution for subsequent UV-visible spectral measurements on a UV-visible-infrared spectrometer (PerkinElmer, Lambda750). Raman and PL spectra were measured on a micro-Raman system (Horiba Jobin Yvon, LabRAM HR 800) with a 514 nm excitation laser. The Raman and PL images were obtained with a confocal micro-Raman system (WITec, Alpha 300a) with a 532 nm laser. The spatial resolution is approximately 250 nm with a focused laser by a 100× objective lens. The time-resolved PL decay transients were measured with a transient state fluorescence spectrometer (HORIBA Jobin Yvon, FL-TCSPC). Chemical composition analysis was performed using XPS (KRATOS Analytical, AXIS Ultra DLD). The surface morphology of the samples was examined by SEM (FEI, Quanta 200FEG) and AFM (Bruker, Dimension Icon). The microstructures of MoS₂ and GQDs were investigated using HRTEM (FEI, Tecnai G2 F20). For the preparation of the TEM samples, the MoS₂ film was also wet-transferred onto TEM grids.

Fabrication of the phototransistors. The phototransistors were fabricated directly on SiO₂/Si substrates after material growth. The SiO₂/Si substrate consists of an oxidation layer (thickness: 300 nm) and highly doped *n*-type silicon, which serves as the back gate electrode. A typical device fabrication process involves UV lithography to define the device pattern and electron-beam evaporation to deposit the source and drain electrodes (*i.e.*, 100 nm Au on top of 5 nm Ti). The GQDs solution was drop-casted onto the MoS₂ phototransistor device followed by a gentle heat treatment at 70 °C for 15 min.

Photoelectrical measurements. Photoelectrical measurements were performed on a probe station (Cascade M150) equipped with a semiconductor property analyser (Keithley 2400) at room temperature in ambient conditions. A tapered optical fibre connected with laser diodes (405 nm, 532 nm and 635 nm) was used to capture the illumination of the photodetector devices. The area size of the laser illumination is much larger than the detection area of the devices (~70000 μm²). The excitation light power mentioned in this work is referred to the actual light power shining onto the device.

References

1. Chhowalla, M. *et al.* The chemistry of two-dimensional layered transition metal dichalcogenide nanosheets. *Nat. Chem.* **5**, 263–275 (2013).
2. Wang, Q. H., Kalantar Zadeh, K., Kis, A., Coleman, J. N. & Strano, M. S. Electronics and optoelectronics of two-dimensional transition metal dichalcogenides. *Nat. Nanotechnol.* **7**, 699–712 (2012).
3. Mak, K. F., Lee, C., Hone, J., Shan, J. & Heinz, T. F. Atomically thin MoS₂: a new direct-gap semiconductor. *Phys. Rev. Lett.* **105**, 136805 (2010).
4. Splendiani, A. *et al.* Emerging photoluminescence in monolayer MoS₂. *Nano Lett.* **10**, 1271–1275 (2010).
5. Radisavljevic, B., Radenovic, A., Brivio, J., Giacometti, V. & Kis, A. Single-layer MoS₂ transistors. *Nat. Nanotechnol.* **6**, 147–150 (2011).
6. Wang, H. *et al.* Integrated circuits based on bilayer MoS₂ transistors. *Nano Lett.* **12**, 4674–4680 (2012).
7. Ji, Q. *et al.* Epitaxial monolayer MoS₂ on mica with novel photoluminescence. *Nano Lett.* **13**, 3870–3877 (2013).
8. Deng, Y. *et al.* Black phosphorus-monolayer MoS₂ van der waals heterojunction p-n diode. *ACS Nano* **8**, 8292–8299 (2014).
9. Jariwala, D. *et al.* Gate-tunable carbon nanotube-MoS₂ heterojunction pn diode. *Proc. Natl. Acad. Sci. USA.* **110**, 18076–18080 (2013).
10. Lopez Sanchez, O., Lembke, D., Kayci, M., Radenovic, A. & Kis, A. Ultrasensitive photodetectors based on monolayer MoS₂. *Nat. Nanotechnol.* **8**, 497–501 (2013).
11. Zhang, W. *et al.* High-gain phototransistors based on a CVD MoS₂ monolayer. *Adv. Mater.* **25**, 3456–3461 (2013).
12. Choi, W. *et al.* High-detectivity multilayer MoS₂ phototransistors with spectral response from ultraviolet to infrared. *Adv. Mater.* **24**, 5832–5836 (2012).
13. Yin, Z. *et al.* Single-layer MoS₂ phototransistors. *ACS Nano* **6**, 74–80 (2011).
14. Lee, H. S. *et al.* MoS₂ nanosheet phototransistors with thickness-modulated optical energy gap. *Nano Lett.* **12**, 3695–3700 (2012).
15. Tsai, D. S. *et al.* Few-layer MoS₂ with high broadband photogain and fast optical switching for use in harsh environments. *ACS Nano* **7**, 3905–3911 (2013).
16. Mueller, T., Xia, F. & Avouris, P. Graphene photodetectors for high-speed optical communications. *Nat. Photonics* **4**, 297–301 (2010).
17. Molina Sanchez, A. & Wirtz, L. Phonons in single-layer and few-layer MoS₂ and WS₂. *Phys. Rev. B* **84**, 155413 (2011).
18. Natori, K. Ballistic metal-oxide-semiconductor field effect transistor. *J. Appl. Phys.* **76**, 4879–4890 (1994).
19. Zhan, Y., Liu, Z., Najmaei, S., Ajayan, P. M. & Lou, J. Large-area vapor-phase growth and characterization of MoS₂ atomic layers on a SiO₂ substrate. *Small* **8**, 966–971 (2012).
20. Liu, K. K. *et al.* Growth of large-area and highly crystalline MoS₂ thin layers on insulating substrates. *Nano Lett.* **12**, 1538–1544 (2012).
21. Lee, Y. H. *et al.* Synthesis of large-area MoS₂ atomic layers with chemical vapor deposition. *Adv. Mater.* **24**, 2320–2325 (2012).
22. Yu, Y. *et al.* Controlled scalable synthesis of uniform, high-quality monolayer and few-layer MoS₂ films. *Sci. Rep.* **3**, 1866 (2013).
23. Tang, L. *et al.* Deep ultraviolet photoluminescence of water-soluble self-passivated graphene quantum dots. *ACS Nano* **6**, 5102–5110 (2012).
24. Luk, C., Chen, B., Teng, K., Tang, L. & Lau, S. Optically and electrically tunable graphene quantum dot-polyaniline composite films. *J. Mater. Chem. C* **2**, 4526–4532 (2014).

25. Tang, L. *et al.* Deep ultraviolet to near-infrared emission and photoresponse in layered n-doped graphene quantum dots. *ACS Nano* **8**, 6312–6320 (2014).
26. Qu, D. *et al.* Formation mechanism and optimization of highly luminescent n-doped graphene quantum dots. *Sci. Rep.* **4**, 5294 (2014).
27. Late, D. J., Liu, B., Matte, H., Rao, C. & Druvid, V. P. Rapid characterization of ultrathin layers of chalcogenides on SiO₂/Si substrates. *Adv. Funct. Mater.* **22**, 1894–1905 (2012).
28. Lee, C. *et al.* Anomalous lattice vibrations of single- and few-layer MoS₂. *ACS Nano* **4**, 2695–2700 (2010).
29. Li, H. *et al.* From bulk to monolayer MoS₂: evolution of Raman scattering. *Adv. Funct. Mater.* **22**, 1385–1390 (2012).
30. Zhang, X. *et al.* Raman spectroscopy of shear and layer breathing modes in multilayer MoS₂. *Phys. Rev. B* **87**, 115413 (2013).
31. Wang, X., Feng, H., Wu, Y. & Jiao, L. Controlled synthesis of highly crystalline MoS₂ flakes by chemical vapor deposition. *J. Am. Chem. Soc.* **135**, 5304–5307 (2013).
32. Chang, Y. H. *et al.* Monolayer MoSe₂ grown by chemical vapor deposition for fast photodetection. *ACS Nano* **8**, 8582–8590 (2014).
33. Konstantatos, G. *et al.* Hybrid graphene-quantum dot phototransistors with ultrahigh gain. *Nat. Nanotechnol.* **7**, 363–368 (2012).
34. Roy, K. *et al.* Graphene-MoS₂ hybrid structures for multifunctional photoresponsive memory devices. *Nat. Nanotechnol.* **8**, 826–830 (2013).
35. Zhang, W. *et al.* Ultrahigh-gain photodetectors based on atomically thin graphene-MoS₂ heterostructures. *Sci. Rep.* **4**, 3826 (2014).
36. Schlaf, R., Lang, O., Pettenkofer, C. & Jaegermann, W. Band lineup of layered semiconductor heterointerfaces prepared by van der Waals epitaxy: Charge transfer correction term for the electron affinity rule. *J. Appl. Phys.* **85**, 2732–2753 (1999).
37. Lee, K. *et al.* Electrical characteristics of molybdenum disulfide flakes produced by liquid exfoliation. *Adv. Mater.* **23**, 4178–4182 (2011).
38. Mahatha, S., Patel, K. & Menon, K. S. Electronic structure investigation of MoS₂ and MoSe₂ using angle-resolved photoemission spectroscopy and ab initio band structure studies. *J. Phys.: Condens. Matter.* **24**, 475504 (2012).
39. Jin, S. H., Kim, D. H., Jun, G. H., Hong, S. H. & Jeon, S. Tuning the photoluminescence of graphene quantum dots through the charge transfer effect of functional groups. *ACS Nano* **7**, 1239–1245 (2013).

Acknowledgements

We acknowledge the support from the National High Technology Research and Development Program of China (863 Program) (Grant No. 2013AA031903), the youth 973 program (2015CB932700), the National Natural Science Foundation of China (Grant No. 51222208, 51290273, 91433107), the Doctoral Fund of Ministry of Education of China (Grant No. 20123201120026), ARC DECRA (DE120101569), DP (DP140101501) and the Engineering Seed Funding Scheme from Monash University. This work was performed in part at the Melbourne Centre for Nanofabrication (MCN) in the Victorian Node of the Australian National Fabrication Facility (ANFF). S. Lin acknowledges the support from the Postdoctoral Science Foundation of China (No. 7131701013), Hong Kong Scholars Program (No. G-YZ36) and the postdoctoral early development program of Soochow University (No. 32317156 & No. 32317267).

Author Contributions

C.C., H.Q. and S.L. contributed equally to this work. Q.B. conceived the idea and supervised the project. C.C., Y.X., J.Y. and W.Y. contributed to synthesis and characterization of MoS₂. H.Q., Y.L., Z.X. and J.S. contributed to device fabrication. S.L., C.M.L. and S.P.L. contributed to preparation of graphene quantum dots. D.L. and C.P. contributed to materials characterization. The manuscript was written by Q.B., C.C. and H.Q. with contributions from all authors. All authors have reviewed the manuscript and given their approval to the final version of this manuscript.

Additional Information

Supplementary information accompanies this paper at <http://www.nature.com/srep>

Competing financial interests: The authors declare no competing financial interests.

How to cite this article: Chen, C. *et al.* Highly responsive MoS₂ photodetectors enhanced by graphene quantum dots. *Sci. Rep.* **5**, 11830; doi: 10.1038/srep11830 (2015).



This work is licensed under a Creative Commons Attribution 4.0 International License. The images or other third party material in this article are included in the article's Creative Commons license, unless indicated otherwise in the credit line; if the material is not included under the Creative Commons license, users will need to obtain permission from the license holder to reproduce the material. To view a copy of this license, visit <http://creativecommons.org/licenses/by/4.0/>